Effect of Temperature and FEC on Silicon Anode Heat Generation Measured by Isothermal Microcalorimetry

View the article online for updates and enhancements.

Effect of Temperature and FEC on Silicon Anode Heat Generation Measured by Isothermal Microcalorimetry

David J. Arnot,[ ] Eric Allcorn,[z] and Katharine L. Harrison

Sandia National Laboratories, Albuquerque, New Mexico 87185, United States of America

Isothermal microcalorimetry (IMC) was used to better understand parasitic reactions and heat generation from Si electrodes in the first 10 cycles using Li/Si half cells. Heat generation from cell polarization (ohmic heat), entropy changes (reversible heat), and parasitic reactions (parasitic heat) are separated and quantified. The effect of temperature and fluoroethylene carbonate (FEC) as an electrolyte additive are also explored. Our results show that at the C/10 cycling rate used here, ohmic heat makes the largest contribution to overall heat generation while reversible heat is the smallest. Ohmic heat generation increases with cycle number due to increasing internal resistance, though the effect is smaller for cells with FEC. Interestingly, capacity-normalized parasitic heat generation is largely unaffected by changes in temperature despite differing reaction kinetics. We show that this is caused by a decrease in average parasitic reaction enthalpy as temperature is increased. Further, cells with FEC display higher average parasitic reaction enthalpy than cells without. The average parasitic reaction enthalpies for all the Si electrodes we tested were lower than previously reported values for graphite, indicating that the SEI formed on Si is less stable.
© 2021 The Electrochemical Society ("ECS"). Published on behalf of ECS by IOP Publishing Limited. [DOI: 10.1149/1945-7111/ac315c]

Silicon has attracted significant attention as a possible replacement for graphite as the negative electrode in lithium-ion batteries due to its high theoretical gravimetric capacity, favorable working voltage, abundance, and low toxicity.[1,2] However, commercialization has been hindered by limited cycle life caused by ineffective passivation, increasing cell impedance, and loss of electrical continuity between the current collector and active material.[3–5] When Si is fully lithiated to form $Li_{15}Si_4$, it undergoes a massive volume change of greater than 300%. With continued cycling the Si particles fracture and separate, resulting in decreased capacity and higher internal resistance.[6] Additionally, the cracks expose fresh Si to the electrolyte causing continuous SEI formation over time which also contributes to increasing internal resistance.

To overcome these issues, several approaches have been taken including decreasing particle size,[7] synthesizing structured particles,[8–11] and employing electrolyte additives.[12–14] Perhaps the most commonly used electrolyte additive is fluoroethylene carbonate (FEC) and its effects have been the subject of several studies with results suggesting that FEC plays a sacrificial role and increases Li^+ conductivity compared to control cells through the formation of LiF crystals which disrupt the otherwise dense SEI.[5] FEC has also been linked to surface modification of Si electrodes where oxygen-free polymers and LiF provide more effective passivation than SEI formed from alkyl carbonate electrolytes without FEC.[15–17] More recently, FEC was shown to reduce the temperature sensitivity of Si/graphite composite anodes.[18]

While much is known about SEI formation on Si with and without FEC, there is still an incomplete understanding, particularly with regard to what effects cycling conditions have on parasitic reactions. Isothermal microcalorimetry (IMC) is a valuable technique that can be used to study these reactions through precise heat flow measurements made during cycling. In fact, IMC has previously been utilized to investigate other electrode materials and battery chemistries including graphite symmetric cells,[19] Li/Fe_3O_4,[20] and graphite/NMC442.[21] A recent IMC study examined the first two (de)lithiation cycles of a Si electrode and separated the measured heat flow into ohmic (polarization), reversible (entropic), and parasitic components.[22] Their results showed that the onset of parasitic reactions occurs early in the first lithiation step and that the thermal energy output from the first lithiation is greater than subsequent (de)lithiation steps. The (de)lithiation processes of metallurgical Si have also been examined using IMC, where parasitic reactions and the enthalpy of crystallization of $Li_{15}Si_4$ were

studied.[23] It was shown that parasitic reactions have a larger current than time dependence and that parasitic power increases below 170 mV vs Li/Li^+.

In this work, the heat flow from Si anodes over the first 10 cycles was measured *operando* using IMC. The heat flow measurements were coupled with ancillary data including equilibrium voltage, internal resistance, and entropic changes in the material during (de) lithiation to separate the heat flow into ohmic, reversible, and parasitic components. The effects of FEC as an electrolyte additive and of cell temperature are quantified to give a greater understanding of the observed cycling behavior. The results presented here expand on previous reports using isothermal microcalorimetry to study Li-ion batteries and give further insight into the effect of FEC and temperature on Si anodes.

Experimental

Battery construction.—The cells tested in this work are 2032 coin cells assembled in a dry room operating at a dew point below −50 °C. The Si electrodes are from the Argonne National Laboratory (ANL) Cell Analysis, Modeling, and Prototyping (CAMP) Electrode Library (A018) and consist of 80 wt.% Si (∼150 nm, Paraclete Energy), 10 wt.% carbon black (Timcal C45), and 10 wt.% LiPAA binder coated onto Cu foil at a thickness of 10 μm. The total material loading for these electrodes is 1.10 mg cm^{-2}. All Si electrodes were 0.625 inches in diameter and cycled against Li foil counter electrodes (Albemarle, 0.38 mm thickness) of the same diameter. Li symmetric cells were also constructed. In all cells, one Celgard 2325 separator was used with 125 μl of electrolyte. The base electrolyte (Gen2) consisted of 3:7 ethylene carbonate (EC):ethyl methyl carbonate (EMC) by weight with 1.2 M $LiPF_6$ and the additive electrolyte (Gen2F) had 10 wt.% FEC.

Cycling parameters.—For background cycling experiments not involving the microcalorimeter, cells were cycled on a Maccor Series 4000 multichannel battery tester. A Tenney Environmental temperature test chamber (model TUJR) was used to control temperature. The Si half cells were cycled at a constant current of C/10 with lithiation and delithiation voltage limits of 0.1 and 1.5 V vs Li/Li^+, respectively. Si half cells with Gen2 and Gen2F electrolytes were cycled 10 times at 30 °C, 45 °C, and 70 °C. All cells were tested in duplicate.

Equilibrium potential and internal resistance.—To estimate equilibrium potential as a function of state-of-charge (SOC), hybrid

[z]E-mail: eallcor@sandia.gov

pulse power characterization (HPPC) was used with a 1.5C pulse and 0.75C regeneration step.[24] For cycles 1, 2, 3, and 5, the method was performed every hour during charge and discharge. The equilibrium potential was calculated by averaging the cell voltage measured at the end of the rest step following the 1.5C pulse and 0.75C regeneration steps. The lithiation and delithiation equilibrium potential for a given SOC differ significantly for Si electrodes,[25,26] so the equilibrium potential curve for a given cycle was taken as the average of the lithiation and delithiation curves. Internal resistance was calculated by dividing the change in voltage by the current during the initial 1.5C pulse using Eq. 1,

$$R_{int} = \frac{\Delta E}{\Delta I} \qquad [1]$$

where ΔE is the voltage change during the initial 1.5C pulse and ΔI is the current change during the same period (from rest to 1.5C).

dE/dT determination.—Reversible heat flow is one of the main three heat flow components considered in this work. To measure reversible heat flow, the quantity *dE/dT* must be determined over all SOCs (see Eq. 2 in the Results and Discussion). We determined *dE/dT* at several SOCs during (de)lithiation of cycles 1 and 2, using the cycle 2 data for all subsequent cycles. Li/Si cells were cycled to a specific SOC at 25 °C, and left to rest for 1 h. The oven temperature was then increased to 35 °C, held for 45 min, and subsequently reduced to 15 °C linearly over 30 min. The change in voltage with time, *dE/dt*, and the change in temperature with time, *dT/dt*, were calculated for the period of linear temperature drop from 35 to 15 °C. To remove "background" voltage change, a power-law function was fit to the data in the 1 h rest step and the slope of the fit function during the temperature change was subtracted from the calculated *dE/dt*. The quotient of the quantities *dE/dt* and *dT/dt* yields *dE/dT*. This *dE/dT* data was used for all the cells we studied, as the (de) lithiation reactions are not likely to change over the 30 °C–70 °C temperature range used here. This method is similar to a previous report,[22] and is an alternative to a step-wise method that has also been used.[27]

Microcalorimetry.—A TA Instruments TAM IV microcalorimeter was used for calorimetry measurements. Two different sized calorimeters were utilized. The first calorimeter has a volume of 20 ml with baseline drift below 1 μW d^{-1} and a precision of 300 nW while the second has a volume of 125 ml with baseline drift below 6 μW d^{-1} and a precision of 3 μW. A dynamic correction was applied to the heat flow signal following a method described by Randzio.[28]

The coin cells were placed in custom holders and inserted into the calorimeter where an oil bath held the temperature constant within 0.1 °C of the set point. To limit heat conduction through the battery leads, phosphor bronze cryogenic wire was used instead of standard copper wire, due to its significantly lower thermal conductivity.[19] Microcalorimeter cells were cycled using a Solartron Modulab XM potentiostat in the manner described above.

Results and Discussion

Baseline cycling.—To serve as a standard for comparison, cells were first cycled outside the microcalorimeter with and without the FEC additive at 30 °C, 45 °C, and 70 °C. The lithiation potential limit for cycling was chosen as 100 mV vs Li/Li$^+$ to prevent significant mechanical degradation of Si caused by the formation of crystalline Li$_{15}$Si$_4$ around 70 mV. This mechanical degradation will not be detected by IMC and therefore could skew results. The 100 mV lithiation limit will also more closely represent the Si electrode potential in future full cell studies planned in support of this work. However, the lithiation potential limit also causes the capacities reported here to be relatively low. Figures 1a–1b show the discharge (lithiation) capacity per gram of Si. As expected, the cycle 1 discharge capacity was higher for cells cycled at greater

temperature due to increased electrolyte conductivity and Li$^+$ diffusion rates. Capacity decay was also accelerated for cells at higher temperatures likely because of faster reaction kinetics for SEI formation. However, the capacity decay was slower for cells with the FEC additive, the effect being greater at higher temperatures. As is common for Si electrodes, the first cycle coulombic efficiency was quite low, in the range of 65–85% (Fig. 1c–1d).[3] The cumulative loss of lithiation capacity, based on the difference between charge and discharge capacity, is shown in Fig. S1 (available online at stacks.iop.org/JES/168/110509/mmedia).

Equilibrium voltage, internal resistance, and dE/dT.—Two methods have been put forth in the literature for quantifying parasitic reactions in Li-ion cells. The first method assumes that the reversible heat for a full lithiation/delithiation cycle is zero and therefore relies on high coulombic efficiency.[19] Parasitic heat can be calculated by subtracting the voltage hysteresis (ohmic heat) from the total heat measured for the cycle. While this method works well for graphite electrodes where coulombic efficiency is relatively high even in early cycles, it is not reliable for Si anodes where coulombic efficiency is much lower. To overcome this issue, Housel et al. demonstrated a second method for separating reversible, ohmic, and parasitic heat contributions continuously during cycling using Eq. 2,[22]

$$\frac{dQ_p}{dt} = \frac{dQ}{dt} - I(E_{load} - E_{Eq}) - IT\left(\frac{dE_{Eq}}{dT}\right) \qquad [2]$$

where *dQ$_p$/dt* is the parasitic heat flow, *dQ/dt* is the heat flow measured by the microcalorimeter, *I* is the current, E_{load} is the cell potential under load, E_{Eq} is the equilibrium cell potential, and *T* is the temperature. The second term on the right-hand side of Eq. 2 is the ohmic heat flow and the third term is the reversible heat flow. Note that this analysis ignores the enthalpy of mixing due to concentration gradients in the electrolyte and Si particles. Recent results show that this is a sound assumption for the relatively slow C/ 10 rate used here.[29] The parasitic reaction term will also include heat generated by the Li counter electrode, however, this heat generation was shown to be minimal at 30 °C,[22] and our own test of a Li/Li symmetric cell at 45 °C gave similar results (Fig. S2). The heat generation is particularly low for later cycles.

To determine the ohmic heat, the equilibrium potential, E_{Eq}, must be measured at all SOCs. Due to incomplete passivation on Si electrodes, the OCP will continuously drift over time so that E_{Eq} cannot simply be measured by letting the cell rest for several hours at different SOCs.[30] To overcome this issue, HPPC was performed on duplicate cells with and without FEC at 30 °C, 45 °C, and 70 °C during cycles 1–5. Due to the relatively large difference between OCP for lithiation and delithiation at a given SOC,[25] the equilibrium potential was taken as the average of the charge and discharge HPPC results for a given cycle. Figure 2 displays the cycle 2 results, where equilibrium potential is shown to decrease as temperature is increased.

HPPC can also be used to calculate the internal resistance of the cell, R$_{int}$, using ohms law and dividing the voltage change during the 1.5C pulse by the current change. Using this method, R$_{int}$ was calculated for several SOCs during charge and discharge. The results for cycle 1 are shown in Figs. 3a–3b. During charge, R$_{int}$ was roughly constant until an SOC of ~0.25 (where an SOC of 1 corresponds to "complete" lithiation at the end of a discharge to 100 mV vs Li/Li$^+$). However, as delithiation continued R$_{int}$ increased rapidly, which could be due to the outside of the Si particles delithiating first, leaving the remaining lithiated Si encapsulated with a longer diffusion path. Additionally, pure amorphous Si has been shown to have conductivity 3–4 orders of magnitude lower than Li-Si alloys.[31] R$_{int}$ was generally lower at high temperatures due to higher electrolyte conductivity and faster Li$^+$ diffusion kinetics. While FEC is known to decrease R$_{int}$, the effect appears to be
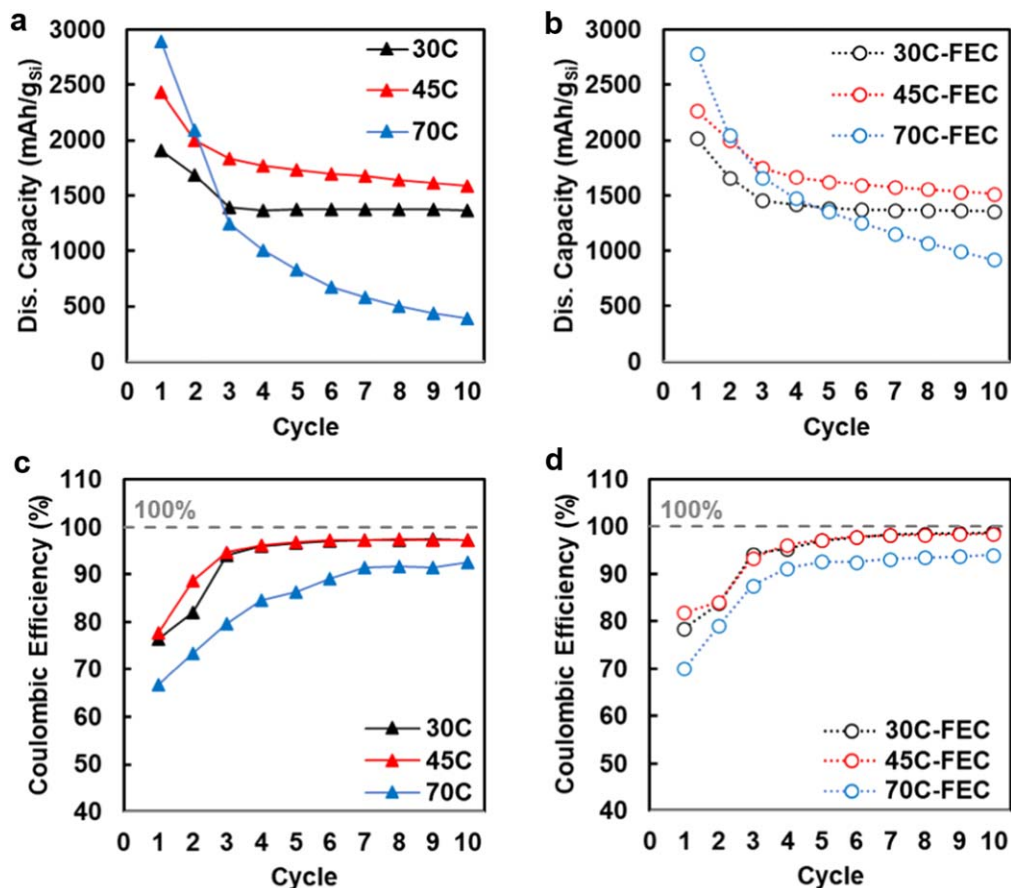
Figure 1. Specific discharge capacity for cells cycled (a) without the FEC additive and (b) with the FEC additive. Coulombic efficiency for cells cycled (c) without the FEC additive and (d) with the FEC additive.
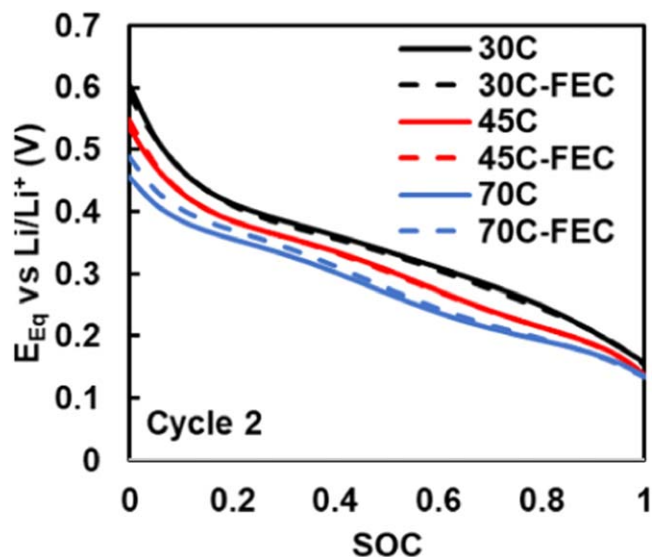

Figure 2. The equilibrium potential, E_{Eq}, determined with HPPC for cells at 30 °C, 45 °C, and 70 °C.

minimal in early cycles where the SEI has not had time to grow significantly.[32] During discharge, R_{int} followed similar trends with regard to temperature and FEC. In this case the high R_{int} at low SOC is not observed because the diffusion distance for Li^+ is short as lithiation begins. R_{int} also tended to decrease as discharge

progressed, consistent with increasing conductivity as the Si is lithiated. This is not surprising because discharge was ended at 100 mV, long before the electrode would be fully lithiated, causing conductivity to decrease.[31]

To demonstrate the trend in R_{int} over the first 5 cycles, Figs. 3c–3d shows values for these cycles at 50% SOC. During charge, R_{int} generally increased with cycle number and FEC showed benefit in the 30 °C and 70 °C cells. Similar to previous reports, the discharge R_{int} for cycle 1 was higher than cycle 2 due to the native oxide layer on the pristine anode being present for cycle 1 but deteriorated after the initial lithiation.[33] In all cases, the largest difference between cells with and without FEC was observed at 30 °C, where slow Li^+ diffusion is likely to have the largest impact on R_{int}.

For reversible heat calculations, the quantity *dE/dT* must be calculated over all lithiation states during charge and discharge.[22] *dE/dT* was measured as outlined in the experimental section and reversible heat flow at C/10 was calculated from those results (Fig. 4). During discharge (lithiation), the reversible heat flow is exothermic and during charge (delithiation), the reversible heat flow is endothermic. Note that the magnitude of the reversible heat flow will increase linearly with the absolute temperature based on Eq. 2. These results are similar to previous reports,[22] with the exception of cycle 1 discharge where differences in starting material crystallinity plays a significant role in entropic changes. The Si used here is largely amorphous as it is designed for high cycle life and to suppress the formation of crystalline phases, which results in the relatively low reversible heat flow observed during the first discharge. The generally flat shape of the reversible heat flow curves indicates that the (de)lithiation reactions don't cause pronounced
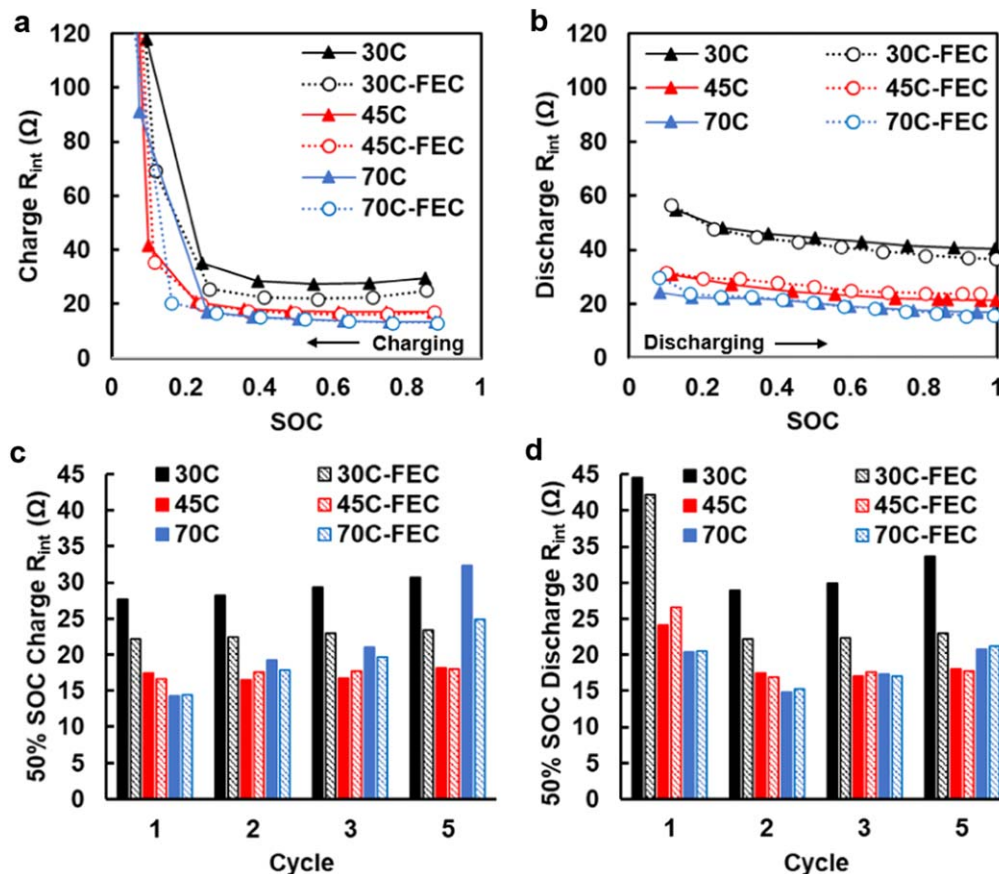
Figure 3. Calculated internal resistance, R_{int}, from HPPC measurements vs SOC for cells during cycle 1 (a) charge and (b) discharge. R_{int} at 50% SOC up to cycle 5 during (c) charge and (d) discharge. R_{int} tends to increase with cycle number due to continuous SEI formation, except for discharge 1, where high R_{int} is caused by a native oxide layer. The FEC additive shows the largest benefit at 30 °C. An SOC of 1 corresponds to a "completely" lithiated electrode at 100 mV vs Li/Li$^+$.

structural changes in the Si as it remains amorphous throughout the potential window used here. This contrasts with entropic changes during graphite lithiation, which correspond to specific phase transitions.[34]

Isothermal microcalorimetry.—Cells with and without FEC were placed inside a microcalorimeter and cycled 10 times at 30 °C, 45 °C, and 70 °C to measure cell heat flow during cycling. Using the method described above, the measured heat flow was split into reversible, ohmic, and parasitic contributions (Fig. S3). Note that reversible heat is positive (exothermic) during discharge and negative (endothermic) during charge, while ohmic and parasitic heat are always positive. Parasitic heat flow is the distance between the measured heat flow line and the summed ohmic and reversible heat flow line. The drastic spike in ohmic heat near the end of charge is consistent with our R_{int} measurements. Parasitic heat is shown to increase at the end of the discharge step, in agreement with previous reports.[23]

It is also useful to compare the thermal energy generation on a total cycle basis for cells cycled under each of the conditions. The nominal heat generation per cycle is shown in Figs. 5a–5b. The significantly higher heat for cycle 1 is due mostly to the initial SEI formation during discharge, but also the high R_{int} of the uncycled Si. Cells with FEC displayed a higher first cycle heat than their non-FEC counterparts, but the difference quickly disappeared, and the values are roughly equal from cycle 2 on. While 30 °C and 45 °C cells had similar total cycle heat generation, 70 °C cells put off much less heat than the others after cycle 2 due to capacity decaying relatively quickly. Perhaps a more informative way of viewing the

data is by normalizing the cycle heat by the cycled capacity (Figs. 5c –5d). In this regard, there is little variation based on temperature, but all cells show slightly increasing cycle specific heat. It is difficult to draw detailed conclusions about heat generation in these cells based only on this data due to competing factors affecting heat generation. For instance, it stands to reason that cells cycled at higher temperature will experience lower overpotentials and therefore less ohmic heat due to higher electrolyte conductivity and faster Li$^+$ diffusion. However, these cells could also experience higher over-potentials from increased current density as the same cycling current is applied to later cycles with less capacity (compared to cells at lower temperatures which have slower capacity decay). Further, cells at higher temperature should also experience higher parasitic heat due to faster reaction kinetics. A more detailed view is required to evaluate these factors and draw meaningful conclusions. We accomplish this by separating ohmic, reversible, and parasitic contributions and combining that information with electrochemical performance details.

The reversible, ohmic, and parasitic heat can also be quantified on a per cycle basis. Figure S4 shows the contributions from each heat source on a nominal and capacity-normalized basis for a cell cycled at 30 °C without FEC as an example. Ohmic heat makes up the majority of heat generation for all cycles followed by parasitic heat. Reversible heat makes up a relatively small portion of the total cycle thermal energy, largely due to cancellation between discharge and charge steps. The total cycle specific reversible heat is shown for all cells in Fig. S5. Since the change in *dE/dT* with SOC is assumed to be constant from cycle 2 on, the reversible heat per cycle is purely a function of the cycled capacity and therefore specific reversible
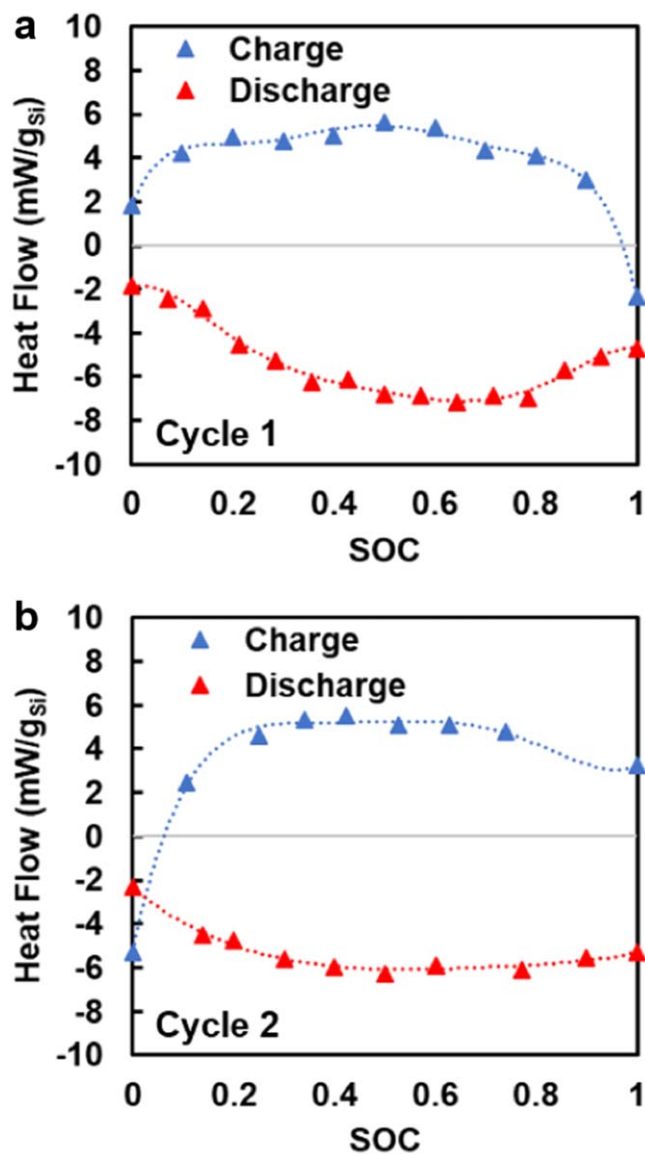
Figure 4. Calculated reversible heat flow during charge and discharge for cells cycled at C/10 and 30 °C for (a) cycle 1 and (b) cycle 2.

heat per cycle will be constant. The shift in specific reversible heat between cells at different temperatures is due to the temperature dependence of reversible heat shown in Eq. 2.

Ohmic heat can also be plotted on a per cycle basis, however, it is more interesting to look at the discharge and charge steps independently (Fig. 6). For the discharge step, ohmic heat remains relatively constant over the first 10 cycles, with the exception of cycle 1 where R_{int} was previously shown to be higher due to the native oxide layer and lower conductivity of pure amorphous Si. Additionally, discharge ohmic heat decreases with increasing temperature, consistent with expectations based on higher electrolyte conductivity and faster Li^+ diffusion. In contrast, during charge the ohmic heat increases with cycle number. The increasing ohmic heat can be attributed to two factors. First, continuous SEI growth will increase R_{int} by forcing Li^+ to diffuse through a longer and more tortuous path. When FEC is present, LiF crystals disrupt the SEI and this results in the lower rate of increase in charge ohmic heat (slope in Fig. 6b) for FEC cells, particularly in cycles 5–10. Second, these cells lose a significant amount of capacity in the first 10 cycles, but the cycling current does not change, resulting in larger overpotentials with each cycle. Since capacity decays faster at higher temperatures, it is

therefore reasonable that charge ohmic heat is higher for cells at higher temperature. What isn't entirely clear is why these effects aren't seen in the discharge ohmic heat as well. One possibility is that this is due to the SEI growing and shrinking cyclically with the (de)lithiation steps (having an overall positive growth rate), referred to as "breathing" in the literature.[35]

With ohmic and reversible heat accounted for, the remaining thermal energy for a given cycle is attributed to parasitic reactions, primarily associated with SEI growth (Fig. 7).[36] There are no clear differences in specific parasitic heat between cells at different temperatures after the first cycle. The fact that significant differences are not observed between temperatures is surprising considering the faster reaction kinetics at higher temperatures which should increase the specific parasitic heat. Lower coulombic efficiency at higher temperatures is also evidence that more parasitic reactions are taking place (mechanical degradation is likely playing a role in the loss of active material as well, however, the relatively high 100 mV cycling limit on the discharge step helps to limit this). To resolve this seeming contradiction, it is important to look at the average parasitic reaction enthalpy.

The average parasitic reaction enthalpy can be calculated by plotting the cumulative parasitic heat generation of the cell against the cumulative moles of Li^+ lost to parasitic reactions (Fig. 8). The cumulative moles of Li^+ lost is calculated as a running total of the difference between charge and discharge capacity for each cycle, where the capacity is converted to moles of Li^+. The reaction enthalpy will be the slope of a linear best-fit line of the data. Due to formation processes occuring in the early cycles, only later cycles where the data points become linear are used. We assume that all capacity loss is related to Si from SEI formation, ignoring any mechanical degradation or passivation of the Li counter electrode. These results suggest that as temperature increases, the average parasitic reaction enthalpy decreases (Table I). This is in agreement with the minimal differences in specific parasitic heat between cells at different temperatures. While the amount of parasitic reactions at higher temperature is greater, the heat generated per reaction is lower.

One implication of the observed decrease in reaction enthalpy is that SEI formed at higher temperatures will be less stable. Further, the average reaction enthalpy of cells with FEC is higher than those without which indicates that the reaction products of the FEC electrolyte are likely more stable. A similar approach has been carried out for graphite, yielding an average parasitic reaction enthalpy of ~212 kJ mol^{-1} at room temperature to form an SEI which is clearly more stable than that of Si.[19] Changes in reaction enthalpy over the temperature range tested here aren't unlikely as electrolytes consisting of organic carbonates with LiPF$_6$ have been shown to degrade at 60 °C–85 °C.[37] A previous report also suggested that electrolyte decomposition products in Si/graphite anodes could differ in the range of 25 °C–55 °C, particularly in the absence of FEC.[18] Our results also show larger differences in this range for cells without FEC as reaction enthalpy drops by ~29% from 30 °C to 45 °C, compared to ~11% for cells with FEC. Further evidence for the stability/reaction enthalpy argument comes from the increase in parasitic power observed at relatively low Si potentials, less than ~170 mV, shown in Fig. S3 and reported previously.[23] This result, coupled with previous work showing greater cycle life for "charge limited" Si electrodes (cycled primarily in a low potential range/highly lithiated state), indicates that the greater parasitic power could be driven, at least in part, by increased average reaction enthalpy and therefore greater stability of the products formed at lower potentials.[16]

Conclusions

Isothermal microcalorimetry was used to study heat generation in Si electrodes over the first 10 (de)lithiation cycles. The effects of temperature and FEC as an electrolyte additive were examined.
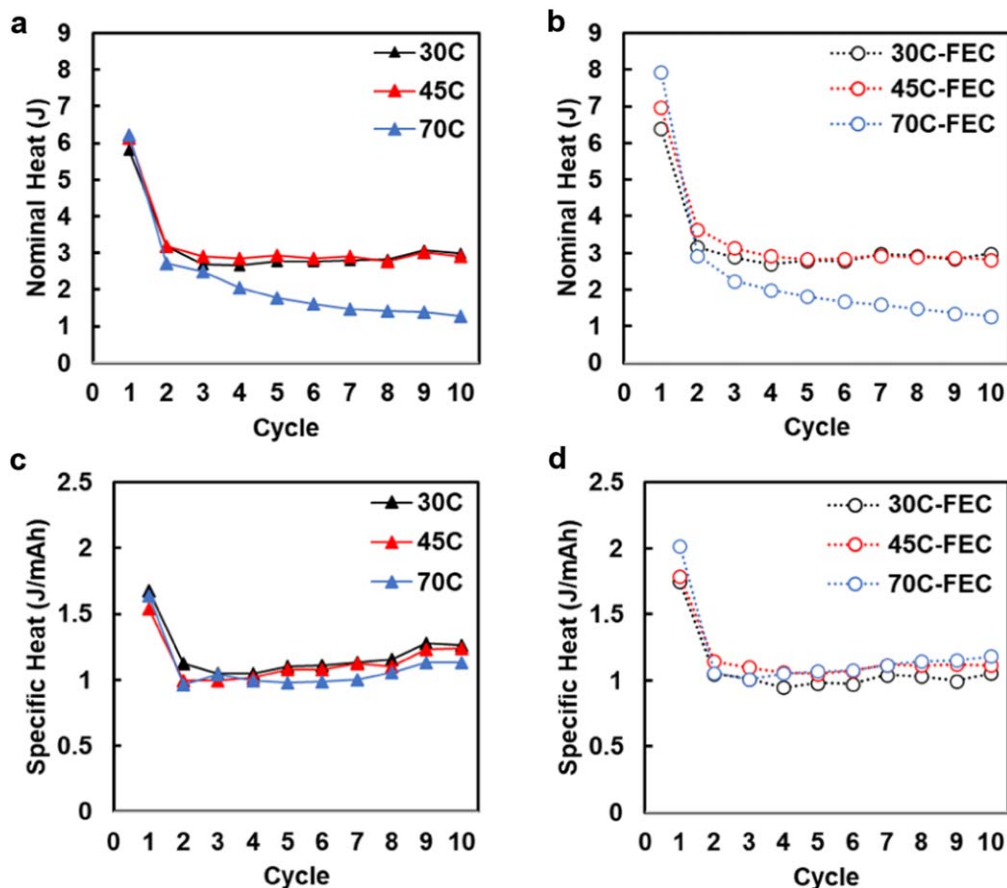
Figure 5. Total cycle nominal heat generation at 30 °C, 45 °C, and 70 °C for cells (a) without FEC and (b) with FEC. Decreasing heat generation from cells cycled at 70 °C is a result of decreasing capacity. Total cycle specific heat generation at 30 °C, 45 °C, and 70 °C for cells (c) without FEC and (d) with FEC.
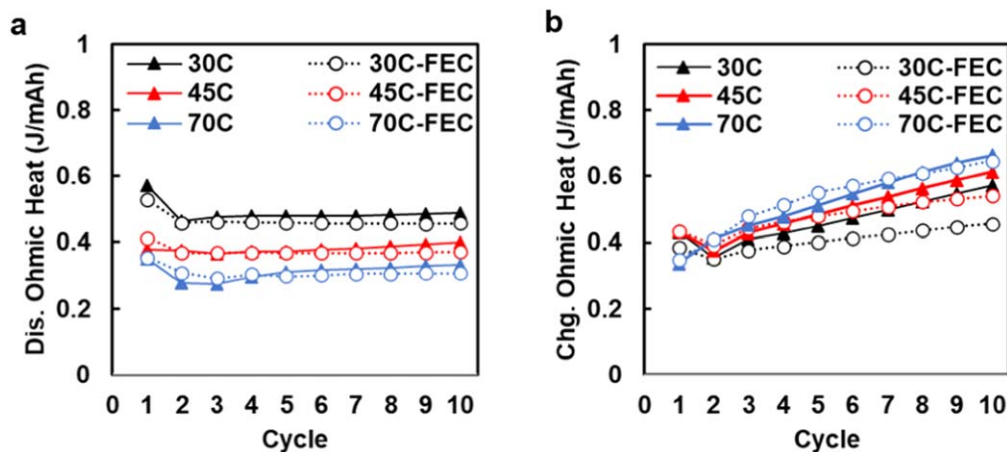
Figure 6. Specific ohmic heat generation for cells cycled at 30 °C, 45 °C, and 70 °C with and without FEC during the (a) discharge step and (b) charge step of a given cycle.

Measurements of equilibrium potential and *dE/dT* over all SOCs allowed for ohmic, reversible, and parasitic heat contributions to be separated. Our results show that ohmic heat represents the greatest contribution to overall heat flow while reversible heat is the smallest. Additionally, discharge ohmic heat flow remains relatively constant after the first cycle while charge ohmic heat flow increases due to increasing charge overpotentials. Consistent with previous reports showing that FEC decreases internal resistance, the increase in charge ohmic heat was slower for cells with FEC. Subtracting ohmic

and reversible heat from the total measured heat yielded the parasitic heat contribution. While specific parasitic heat flow was roughly the same for all temperatures, we show that this is due to lower average reaction enthalpy at higher temperatures which offsets the greater quantity of parasitic reactions. Parasitic reaction enthalpy was found to be greater for cells with FEC, indicating greater SEI stability. Lower average parasitic reaction enthalpy for all cells tested compared to previously studied graphite electrodes indicates that the SEI formed on Si is less stable than the SEI formed on graphite.
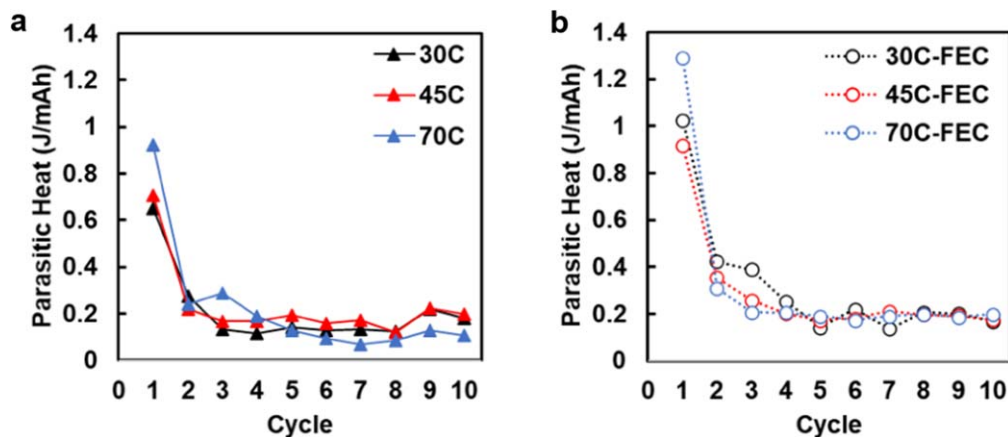
Figure 7. Cycle parasitic heat for cells cycled at 30 °C, 45 °C, and 70 °C (a) without FEC and (b) with FEC.
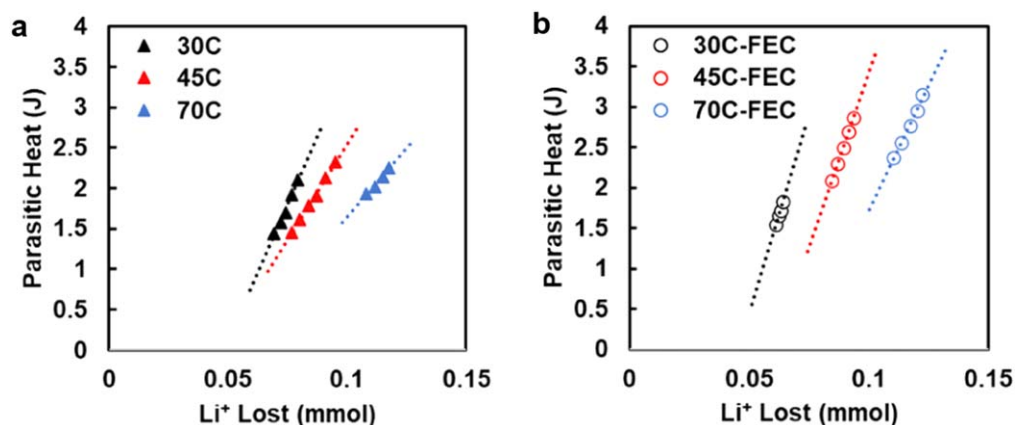

Figure 8. Cumulative parasitic heat vs cumulative mmol of Li$^+$ lost to parasitic reactions for cells at 30 °C, 45 °C, and 70 °C (a) without FEC and (b) with FEC. Only the last cycles where slope becomes linear are shown.

Table I. Average Parasitic Reaction Enthalpies.

Temperature (°C)	ΔH_{rxn} (kJ/mol)
No FEC	
30	62 ± 7
45	44 ± 4
70	31 ± 4
10% FEC	
30	103 ± 7
45	92 ± 6
70	63 ± 1

The results presented here expand on previous studies utilizing isothermal microcalorimetry to study battery materials and give greater insight into the effects of temperature and FEC on Si anodes.

ORCID

David J. Arnot https://orcid.org/0000-0002-1138-3655

References

1. X. Zuo, J. Zhu, P. Müller-Buschbaum, and Y. J. Cheng, *Nano Energy*, **31**, 113 (2017).
2. B. Liang, Y. Liu, and Y. Xu, *J. Power Sources*, **267**, 469 (2014).
3. J. R. Szczech and S. Jin, *Energy Environ. Sci.*, **4**, 56 (2011).
4. A. Franco Gonzalez, N. H. Yang, and R. S. Liu, *J. Phys. Chem. C*, **121**, 27775 (2017).
5. E. Peled and S. Menkin, *J. Electrochem. Soc.*, **164**, 1703 (2017).
6. X. Su, Q. Wu, J. Li, X. Xiao, A. Lott, W. Lu, B. W. Sheldon, and J. Wu, *Adv. Energy Mater.*, **4**, 1300882 (2014).
7. R. Deshpande, Y. T. Cheng, and M. W. Verbrugge, *J. Power Sources*, **195**, 5081 (2010).
8. W. Qi, J. G. Shapter, Q. Wu, T. Yin, G. Gao, and D. Cui, *J. Mater. Chem. A*, **5**, 19521 (2017).
9. C. K. Chan, H. Peng, G. Liu, K. McIlwrath, X. F. Zhang, R. A. Huggins, and Y. Cui, *Nat. Nanotechnol.*, **3**, 31 (2008).
10. N. Liu, H. Wu, M. T. McDowell, Y. Yao, C. Wang, and Y. Cui, *Nano Lett.*, **12**, 3315 (2012).
11. J.-K. Yoo, J. Kim, Y. S. Jung, and K. Kang, *Adv. Mater.*, **24**, 5452 (2012).
12. K. Schroder, J. Alvarado, T. A. Yersak, J. Li, N. Dudney, L. J. Webb, Y. S. Meng, and K. J. Stevenson, *Chem. Mater.*, **27**, 5531 (2015).
13. C. Xu, F. Lindgren, B. Philippe, M. Gorgoi, F. Björefors, K. Edström, and T. Gustafsson, *Chem. Mater.*, **27**, 2591 (2015).
14. T. Jaumann et al., *Energy Storage Mater.*, **6**, 26 (2017).

15. E. Markevich, G. Salitra, and D. Aurbach, *ACS Energy Lett.*, **2**, 1337 (2017).
16. E. Markevich et al., *J. Electrochem. Soc.*, **160**, A1824 (2013).
17. R. Elazari, G. Salitra, G. Gershinsky, A. Garsuch, A. Panchenko, and D. Aurbach, *J. Electrochem. Soc.*, **159**, A1440 (2012).
18. M. J. Piernas-Muñoz, S. E. Trask, A. R. Dunlop, E. Lee, and I. Bloom, *J. Power Sources*, **441** (2019).
19. L. J. Krause, L. D. Jensen, and J. R. Dahn, *J. Electrochem. Soc.*, **159**, A937 (2012).
20. M. M. Huie, D. C. Bock, A. M. Bruck, K. R. Tallman, L. M. Housel, L. Wang, J. Thieme, K. J. Takeuchi, E. S. Takeuchi, and A. C. Marschilok, *ACS Appl. Mater. Interfaces*, **11**, 7074 (2019).
21. L. E. Downie, S. R. Hyatt, A. T. B. Wright, and J. R. Dahn, *J. Phys. Chem. C*, **118**, 29533 (2014).
22. L. M. Housel et al., *ACS Appl. Mater. Interfaces*, **11**, 37567 (2019).
23. V. L. Chevrier, Z. Yan, S. L. Glazier, M. N. Obrovac, and L. J. Krause, *J. Electrochem. Soc.*, **168**, 030504 (2021).
24. A. Barai, K. Uddin, M. Dubarry, L. Somerville, A. McGordon, P. Jennings, and I. Bloom, *Prog. Energy Combust. Sci.*, **72**, 1 (2019).
25. V. A. Sethuraman, V. Srinivasan, and J. Newman, *J. Electrochem. Soc.*, **160**, A394 (2013).
26. V. L. Chevrier and J. R. Dahn, *J. Electrochem. Soc.*, **156**, A454 (2009).
27. N. S. Hudak, L. E. Davis, and G. Nagasubramanian, *J. Electrochem. Soc.*, **162**, A315 (2015).
28. S. L. Randzio and J. Suurkuusk, *Biological Microcalorimetry* (Academic Press, London) 311 (1980).
29. D. Chalise, W. Lu, V. Srinivasan, and R. Prasher, *J. Electrochem. Soc.*, **167**, 090560 (2020).
30. K. Kalaga, M. T. F. Rodrigues, S. E. Trask, I. A. Shkrob, and D. P. Abraham, *Electrochim. Acta*, **280**, 221 (2018).
31. E. Pollak, G. Salitra, V. Baranchugov, and D. Aurbach, *J. Phys. Chem. C*, **111**, 11437 (2007).
32. C. Stetson, Y. Yin, A. Norman, S. P. Harvey, M. Schnabel, C. Ban, C. S. Jiang, S. C. DeCaluwe, and M. Al-Jassim, *J. Power Sources*, **482**, 228946 (2021).
33. J. J. Wu and W. R. Bennett, *2012 IEEE Energytech, Energytech 2012* (2012).
34. D. Allart, M. Montaru, and H. Gualous, *J. Electrochem. Soc.*, **165**, A380 (2018).
35. G. M. Veith, M. Doucet, R. L. Sacci, B. Vacaliuc, J. K. Baldwin, and J. F. Browning, *Sci Rep.*, **7**, 1 (2017).
36. S. Chae, W. J. Kwak, K. S. Han, S. Li, M. H. Engelhard, J. Hu, C. Wang, X. Li, and J. G. Zhang, *ACS Energy Lett.*, **6**, 387 (2021).
37. B. Ravdel, K. M. Abraham, R. Gitzendanner, J. DiCarlo, B. Lucht, and C. Campion, *J. Power Sources*, **119–121**, 805 (2003).